Wind tunnel validation of AeroDyn within LIFES50+ project: imposed Surge and Pitch tests

You may also be interested in:

On the functional design of the DTU10 MW wind turbine scale model of LIFES50+ project
I. Bayati, M. Belloli, L. Bernini et al.

Wind tunnel validation of AeroDyn within LIFES50+ project: imposed Surge and Pitch tests

I. Bayati[1*]**, M. Belloli**[1]**, L. Bernini**[1]**, A.Zasso**[1]

[1]Politecnico di Milano, Department of Mechanical Engineering, Milan, Italy

E-mail: `ilmasandrea.bayati@polimi.it` *, `marco.belloli@polimi.it`,
`luca.bernini@polimi.it`, `alberto.zasso@polimi.it`

Abstract. This paper presents the first set of results of the steady and unsteady wind tunnel tests, performed at Politecnico di Milano wind tunnel, on a 1/75 rigid scale model of the DTU 10 MW wind turbine, within the LIFES50+ project. The aim of these tests is the validation of the open source code AeroDyn developed at NREL. Numerical and experimental steady results are compared in terms of thrust and torque coefficients, showing good agreement, as well as for unsteady measurements gathered with a 2 degree-of-freedom test rig, capable of imposing the displacements at the base of the model, and providing the surge and pitch motion of the floating offshore wind turbine (FOWT) scale model. The measurements of the unsteady test configuration are compared with AeroDyn/Dynin module results, implementing the generalized dynamic wake (GDW) model. Numerical and experimental comparison showed similar behaviours in terms of non linear hysteresis, however some discrepancies are herein reported and need further data analysis and interpretations about the aerodynamic integral quantities, with a special attention to the physics of the unsteady phenomenon.

1. Introduction

Lifes50+ is an EU H2020 project which aims at proving cost effective technology for floating substructures for 10MW wind turbines, at water depths greater than 50 m. The objective is optimizing and qualifying to a Technology Readiness Level (TRL) of 5, i.e. technology validated in relevant environment, two innovative substructure designs for 10MW wind turbines, as well as, developing a methodology for the evaluation process of floating substructures. For this project, the reference 10 MW wind turbine developed by DTU [1] is taken as reference for numerical and experimental studies.

Furthermore, the aerodynamics of FOWT has a particular unsteady nature, due to the motion of the platform causing non-negligible variation in the incoming wind speed and angle of attack seen by the blade airfoils. Therefore, the rotor experiences dynamic extra loads, that affect the overall dynamics of the system, which is worthy of experimental investigation through wave basin and wind tunnel tests.

More specifically, Lifes50+ [2] implements a novel experimental approach to test floating wind turbines, with the main goal of overcoming the scaling issues, typically associated to system simultaneously loaded by wind and waves, such as the Froude/Reynolds conflict related to the impossibility of ensuring both Froude and Reynolds numbers similitude. In order to take the advantages from both wave basin and wind tunnel facilities and to perform more reliable tests, the approach consists in the "Hardware-In-The-Loop" hybrid testing, where the model is subjected both to experimentally measured and numerically computed forces, in real time. In the wave basin, the real-time forcing system is a set of fish lines with spring in series actuated by electrical motors (force control), reproducing aerodynamic forces [3]. In the wind tunnel, a 2 degree-of-freedom (DoF) [4] or 6 DoF robot [5], provides the motion to the wind turbine model (motion control).

In this paper the results of an experimental campaign, carried out at Politecnico di Milano Wind Tunnel, aimed at assessing the influence of the offshore wind turbine motion on the aerodynamic loads, are reported. More specifically, a 2DoF mechanical system was adopted to impose the surge and pitch motion to the wind turbine model. The motion provided were mono-harmonic sinusoidal displacements at the base of the tower, by means of hydraulic actuators, as shown in Fig.1 and 2. Reasonable amplitudes and frequencies, both in the low and wave frequency ranges for a 10MW machine, were considered during the test.
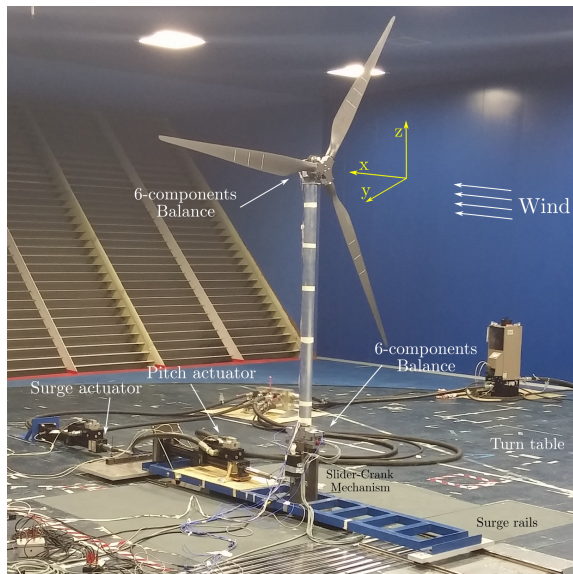

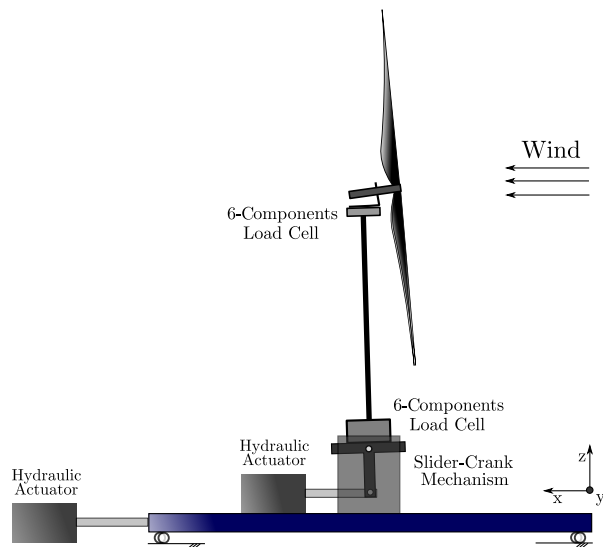Figure 1: 1/75 DTU 10 MW reference wind turbine [1]

Figure 2: 2 Degrees-of-Freedom (Surge and Pitch) Test Rig

2. Wind Turbine Model

The wind turbine model is a rigid one, with 1/75 length scale factor. It was tested in the Atmospheric Boundary Layer (ABL) test section of Politecnico di Milano Wind Tunnel, whose dimensions are 13.84 m x 3.84 m. Although the focus of the present paper is much more on the results of the wind tunnel experimental campaign, rather than the blades and nacelle design, which are more thoroughly treated respectively in [6] and [7], a brief description of the main features is herein reported. More specifically, in Tab.1 the scaling factors adopted to build the model are reported following the definition λ = full scale/model. Once defined the length and speed scale factors, respectively $\lambda_L = 75$ and $\lambda_V = 3$, all the other quantities were consistently derived [10]. The choice of λ_L value is basically reflecting the desire of finding an optimal compromise between maximizing the dimensions for lowering the Reynolds mismatch and limiting the dimensions to limit the blockage ratio, around 8%, being the effective rotor diameter D = 2.36 m. Concerning the λ_V, the aerodynamic design reported in [6] was developed for $\lambda_V = 2$ considered a good compromise keeping into account the maximum wind tunnel wind speed and the full scale cut off. Results both for $\lambda_V = 2$ and $\lambda_V = 3$ are herein reported for the steady tests. However, only $\lambda_V = 3$ tests are reported for the unsteady ones, since they turned out to be preferable, because of lower frequencies of the surge and pitch imposed motion, with respect to $\lambda_V = 2$ (i.e. λ_f, Tab.1). For the rigid version of the wind turbine model, which has been used for this test session, the blades have been realized, after an extensive design and testing preliminary campaign, with the scope of matching the target scaled thrust force (λ_F), for its importance in the dynamics of FOWT. Similar previous experience in aerodynamic scaling and blade manufacturing of wind turbines can be found in [9], [10], [11], dealing with the typical scaling issues. With regard to blade aerodynamics, switching from the full scale wind turbine to the scaled model requires the usage of Low-Reynolds fitted profiles. This is due to the high full-scale/wind tunnel discrepancy in the Reynolds number (approximately 150), which drives the aerodynamics. More

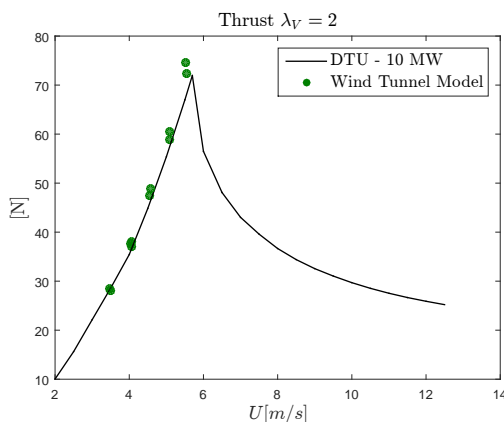| Quantity	Scaling Rule	Scale Factors	
Length	λ_L	75	75
Speed	λ_V	2	3
Rotor speed	$\lambda_\omega = \lambda_V/\lambda_L$	1 : 37.5	1 : 25
Frequency	$\lambda_f = \lambda_V/\lambda_L$	1 : 37.5	1 : 25
Time	$\lambda_T = \lambda_L/\lambda_V$	37.5	25
Acceleration	$\lambda_{acc} = \lambda_L\lambda_f^2$	1 : 18.75	1 : 8.34
Force	$\lambda_F = \lambda_V^2\lambda_L^2$	22500	50625
Mass	$\lambda_M = \lambda_L^3$	421875	421875

Table 1: Scaling Factors

Figure 3: Thrust for $\lambda_V = 2$: DTU10 MW reference Vs PoliMi Wind Tunnel Model

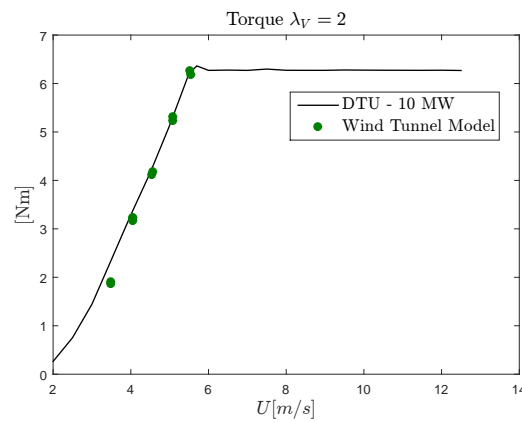

Figure 4: Torque for $\lambda_V = 2$: DTU10 MW reference Vs PoliMi Wind Tunnel Model

specifically, a SD7032 airfoil was eventually adopted, based on Selig database [12]. Before designing the final blade, a sectional test campaign in the DTU red wind tunnel was performed. Aim of these preliminary tests was to check the consistency of the effective airfoil, with the adopted manufacturing process, with the Selig database, in terms of lift and drag coefficients C_l and C_d. To this aim the SD7032 section blade, was tested within the Reynolds number range [`5E4` - `2.5E5`], equipping the model also with pressure taps, force gauges and measuring the wake, studying the influence of turbulators, as well. The lift and drag coefficients C_L and C_D where respectively derived from the pressure and wake measurements and were adopted as reference for the design of the blades, as explained in [6].

For this test session ([2]) a fixed-pitch version of the wind turbine was used, so that the pitch was varied manually by a very fine gear reduction system to set the nominal pitch angle of the blade.

3. Steady results
In this section the results about the steady tests, aimed at characterizing the performance of the scaled machine along the reference curve, are here reported. More specifically in Fig.3 - 8, results are reported, both for $\lambda_V = 2$ and $\lambda_V = 3$, in terms of rotor thrust, torque and thrust coefficient C_t. It can be noticed that correct thrust target-oriented aerodynamic design [6] ($\lambda_V = 2$) is evidently reached, both in terms of thrust and torque up to rated condition (Fig.3, 4 and 7). Regarding the above rated conditions, it is worth mentioning that these tests were conducted considering the DTU 10 MW [1] reference conditions also in terms of pitch angle. Therefore in Fig.3 - 8 the points up to rated conditions are characterized by a 0° pitch angle. However, having the possibility of changing the pitch angle by means of miniaturized servo-actuators for Individual Pitch Control (IPC), available in the wind tunnel model being finalized, see [7], will be used to properly tune the pitch angle to reach the desired values of the aerodynamic forces,
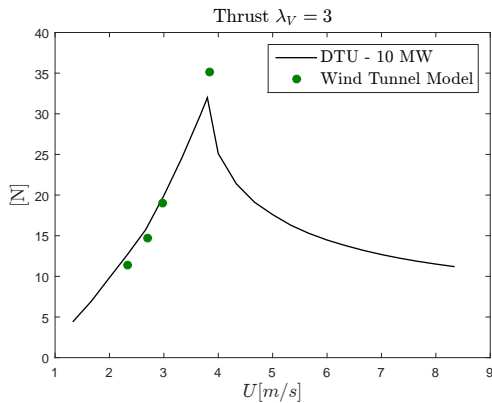
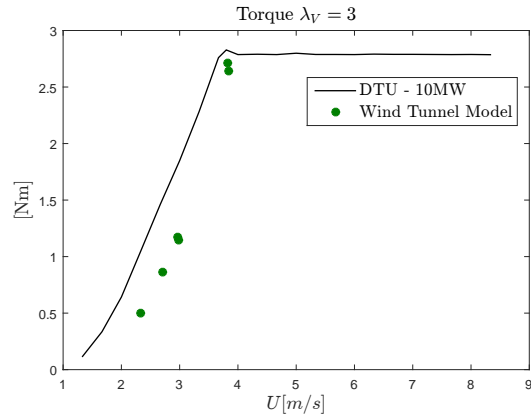Figure 5: Thrust force for $\lambda_V = 3$: DTU10 MW reference Vs PoliMi Wind Tunnel Model

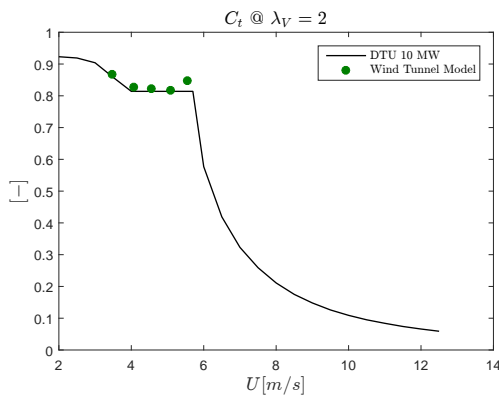Figure 6: Torque for $\lambda_V = 3$: DTU10 MW reference Vs PoliMi Wind Tunnel Model

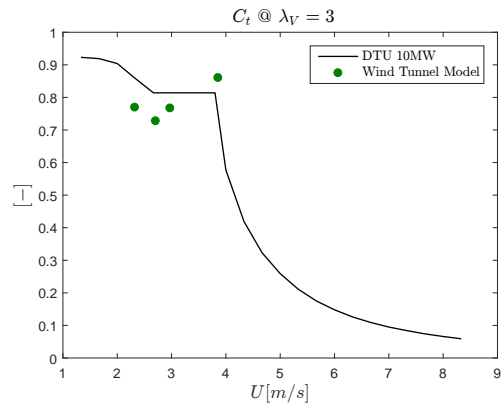Figure 7: Thrust coefficient for $\lambda_V = 2$: DTU10 MW reference Vs PoliMi Wind Tunnel Model

Figure 8: Thrust coefficient for $\lambda_V = 3$: DTU10 MW reference Vs PoliMi Wind Tunnel Model

below and above rated conditions. For the wind tunnel assessment of the dynamics of FOWT, the results for $\lambda_V = 2$ can be considered already excellent, consistently with the design. For $\lambda_V = 3$ the results are very good, with a potential improvement by the usage of turbulators, which are supposed to decrease the additional drag due to laminar separation bubbles in low speed regimes, and by tuning by fine blade pitch regulation, for Reynolds regimes slightly different from the design one (i.e. $\lambda_V = 2$).

4. Unsteady tests and data analysis approach
As visible in Fig. 2 the test rig consists in a 2 DoF mechanical system. More specifically, the wind turbine scaled model is mounted to this mechanism by means of a 6-components load cell to measure the forces at the base of the tower (RUAG/192-6I). Another smaller 6-components load cell is mounted between the nacelle and the tower (Fig.1). Furthermore, all the electrical quantities regarding the brushless motor are measured. In Fig.2 is clear how the imposed surge and pitch motions are provided to the wind turbine model. Two hydraulic actuators (MTS 244.11) are servo-driven pushing a slider (surge), as well as a slider-crank mechanism translating the linear displacement to a rotation (pitch).

As a matter of fact, for a given wind speed, imposing the motion of the wind turbine ends up in measuring forces which are composed by a significant inertial contribution along with the aerodynamic component, which is the final goal of these tests. Therefore, each test was repeated twice with the wind respectively "turned off" and "on"; this led to the identification of the effective mass and moment of inertia associated to each motion condition. These quantities are used to compute the inertial forces used to

compute the pure aerodynamic loads. The operation inertial force subtraction is not that straightforward, as it deals with time histories coming from different instruments, so there can be a phase lag between each.Therefore, the forces were treated by means of a precise procedure that can be summarized as follows:

(i) realignment of time series based on the motion frequency band-pass filtered signal of the actuators displacement (hydraulic actuators LVDT sensors), by detecting the zero crossing points

(ii) detection of the displacement fundamental harmonic contribution from the force signals

- implementation of the Fast Fourier Transform (FFT)
- detection of the exact peak in the frequency domain
- reconstruction of the time domain fundamental force signal through Inverse Fast Fourier Transform (IFFT)

(iii) computation of the aerodynamic force $F_{Aero} = F_{Tot} - F_{Inertial}$

more details can be found in [13]. More specifically, in order to have the highest precision as possible in the computation of the FFT, the sampling frequency and the acquisition time window were chosen so that a finite number of period of motion were gathered. In Fig.9 an overview of the data processing is reported.
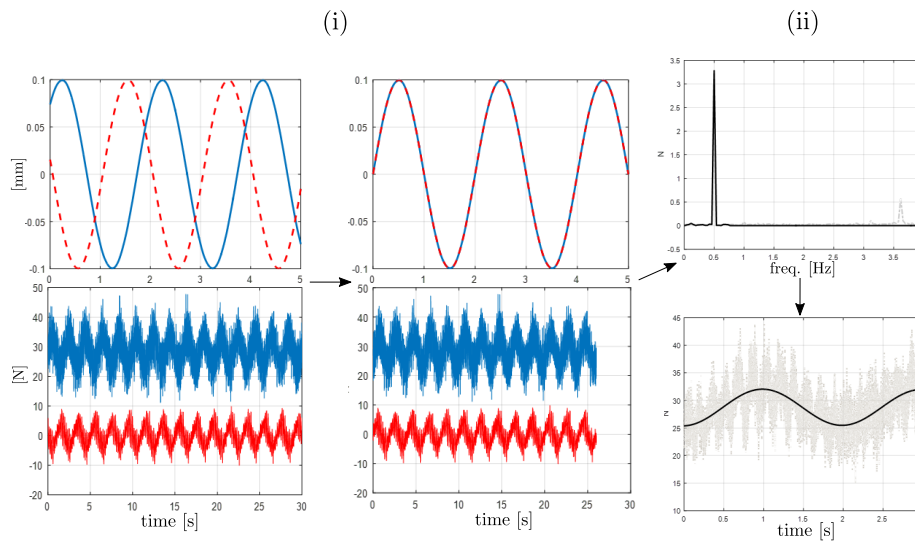

Figure 9: Flowchart for the data process leading the detection of aerodynamic force only from the imposed motion tests.

5. FAST-HydroDyn custom version

In order to compare AeroDyn output with the experimental results, the same numerical environment was to be set up. To this aim, previous versions of FAST (i.e. v7) were capable to provide imposed force at the base of onshore wind turbines (i.e. Seismic module). However, this functionality has not been updated any longer in the recent NREL/FAST releases. Therefore, a custom version of FAST (v8/AeroDyn v.13) was compiled, giving the possibility to the user to define surge and pitch sine motion, specifying amplitude and frequency. These are treated as target motion at the base of the tower, so that they are achieved through a feedback control force, based on user defined proportional and derivative gain constants [K] and [C], see Eq.1, which can be properly tuned to obtain the desired motion $\underline{X}_{Ref}$:

$$\underline{F}_{Base} = [K](\underline{X}_{Ref} - \underline{X}_{Eff}) + [C](\underline{\dot{X}}_{Ref} - \underline{\dot{X}}_{Eff}) \tag{1}$$

Moreover, the simulation settings that were run with this FAST v8 custom version for the comparison with the experimental results are reported in Tab.2. It can be noticed that the simulations were run setting Dynin inflow model, which implements Generalized Dynamic Wake Model (GDW), suitable for representing unsteady aerodynamics. Moreover, no dynamic stall model was implemented in FAST at this point, either for the lack of unsteady experimental data on the airfoil sectional model and to investigate if the GDW only was sufficient to predict the experimental results.

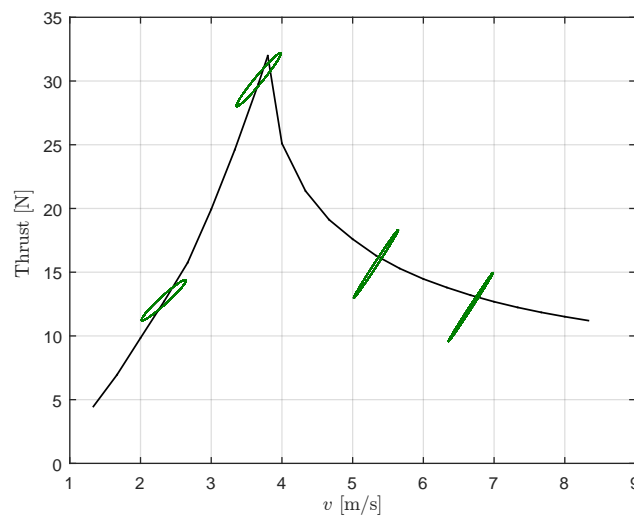| Simulation Parameter	Setting
AeroDyn time step	0.001
Dynamic Stall Model	Steady (no stall modelling)
Use Cm	No
Inflow Model	Dynin (GDW)
Induction factor model	Swirl
Tip Loss Model	Prandtl
Hub Loss Model	Prandtl
Blades	Rigid
Fixed pitch	No controller

Table 2: FAST/AeroDyn simulation settings.

Figure 10: 2 Degrees-of-Freedom (Surge and Pitch) Test Rig

6. Unsteady Results

As previously mentioned, the aerodynamic thrust was the force mainly investigated out of this wind tunnel experimental campaign and it shows an hysteretic behaviour when represented against the effective wind velocity. A good number of combinations for surge and pitch, in terms of low/wave frequency range up to rated wind condition, were considered in the definition of the test matrix, see Tab.3 and 4; however, the complete test session, can be found in [2]. In Fig.10 a general view is reported about how thrust force qualitatively behaves around the nominal wind velocity. In Fig.10 the two set of hysteresis above rated are to be intended with fixed blades pitch kept as the nominal one.

The comprehension of this first set of results, reported in Fig.13-24 is not obvious and it is still object of investigation by the authors, however, Fig.11 and 12 can be consider a good support to the following

discussion and they represent a straightforward indication about in-phase and quadrature aerodynamic force component. With regard to Fig.11, let us concerned with three different aerodynamic forces, F_1, F_2 and F_3, perfectly in-phase with the effective velocity of the hub, for example. These force have merely growing amplitudes, therefore, representing these as function of the velocity itself implies has a consequent increase in slope. Furthermore, if we consider other three forces F_1, F_2 and F_3 of the same amplitude, but changing the phase shift up to the force F_3 perfectly in quadrature with respect to the velocity (i.e. $\pi/2$ of phase shift), the force Vs velocity corresponding plot turns out to be hysteretic with an increasing area up to a perfect circle. Both in Fig.11 and Fig.12 the i-th force F_i and the velocity U_{Dyn} are intended to be de-trended by the mean value, therefore only the unsteady part is represented (see Fig.10). Since each sine wave can be represented as composed by an in-phase and quadrature components, the unsteady aerodynamic forces will be given as a combination of these two effects (Fig.11 and Fig.12). More specifically, an in-phase component with respect to the velocity means a viscous damping contribution of the aerodynamic forces, whereas a quadrature component is linked to the added mass or aerodynamic stiffness, as more clear in Eq.3. Since every sine imposed motion given to the platform $sin(\omega t)$ produce an aerodynamic force $F_{aero}^{Dyn} = A_F sin(\omega t + \phi)$ with a certain amplitude A and a phase shift ϕ (i.e. transfer function), it can also be always represented as composed of a in-phase (P) and a quadrature (Q) component, as shown in Eq.2:

$$
\begin{aligned}
F_{aero}^{Dyn} = A_F sin(\omega t + \phi) &= A_F cos(\phi)sin(\omega t) + A_F sin(\phi)sin(\omega t + \frac{\pi}{2}) \\
&= A_P \cdot sin(\omega t) + A_Q \cdot sin(\omega t + \pi/2) \\
&= A_P \cdot sin(\omega t) + A_Q \cdot cos(\omega t)
\end{aligned}
\tag{2}
$$

Considering the global dynamic equation of the rigid scale model imposed motion, with respect to the degree of freedom considered (surge or pitch) x, and a linearization about the steady steady aerodynamic force F_0, the contribution A_P and A_Q of the unsteady aerodynamic force can be highlighted:

$$
\begin{aligned}
m\ddot{x} + c\dot{x} + kx &= F_{Aero}(t, x, \dot{x}, \ddot{x}) \\
&= F_0 + \frac{\partial F}{\partial x}\Big|_0 x + \frac{\partial F}{\partial \dot{x}}\Big|_0 \dot{x} + \frac{\partial F}{\partial \ddot{x}}\Big|_0 \ddot{x} + F_0 + k_{aero}x + c_{aero}\dot{x} + m_{aero}\ddot{x} \\
&= F_0 + c_{aero}\dot{x} + (m_{aero} - k_{aero})j\omega\dot{x} = F_0 + A_P\dot{x} + A_Q j\omega\dot{x} \\
&= F_0 + F_{aero}^{Dyn}
\end{aligned}
\tag{3}
$$

where the aerodynamic mass m_{aero}, damping c_{aero} and stiffness k_{aero} are grouped with respect to the velocity $\dot{x}$, also referred to as U_{Dyn} "dynamic wind speed". Therefore, the forces can be represented as vector of components A_P and A_Q in the Gauss diagram (Fig.11-12), giving a straightforward interpretation of the experimental Vs numerical comparison. It is worth noticing that the term A_Q, according to this representation of Eq.3, can be negative if $k_{aero} > m_{aero}$, thus the vector in the Gauss diagram potentially in the fourth quadrant.

In Fig. 13-16 the results for surge imposed motion up to rated condition, where no aerodynamic stall is expected, are reported along with the corresponding vectorial representation in the Gauss diagram. In Tab.3 a summary of results is reported along with some useful adimensional parameters that could be potentially representing all the information regarding the dynamic condition of the wind turbine (wind and wave) being analysed. Similarly for the pitch, in Fig.19-22 and Tab.4.

More specifically the reduced frequency f^* can be defined as the platform imposed velocity ($\omega_p A$) over incoming wind speed U, as in Eq.4:

$$
f^* = \frac{\omega_p A}{U} = \frac{U_{Dyn}}{U}
\tag{4}
$$

where ω_p is the imposed circular frequency and A is the imposed motion amplitude, in m or deg respectively for surge and pitch. In Fig.13 - 16 for surge, and Fig.19 - 22 for pitch, the results up to rated condition are reported both for low frequency (left) and wave frequency (right) hydrodynamic condition; with the terms *wave* and *low* frequencies, respectively the motion components due to wave exciting harmonics within the non-zero wave spectrum frequency range and lower ([14], [15]). The dashed
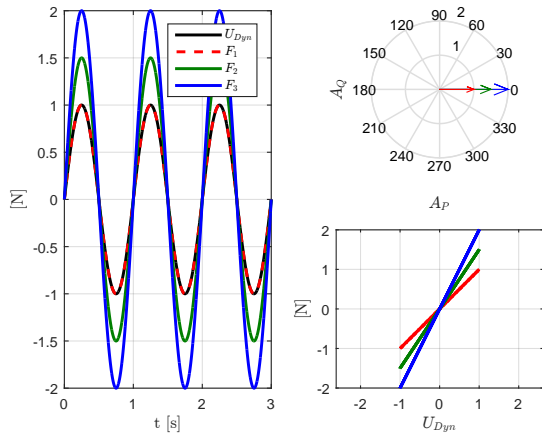
Figure 11: Simple example: effect of **in-phase** component of the aerodynamic force F_i with respect to the velocity U_{Dyn}
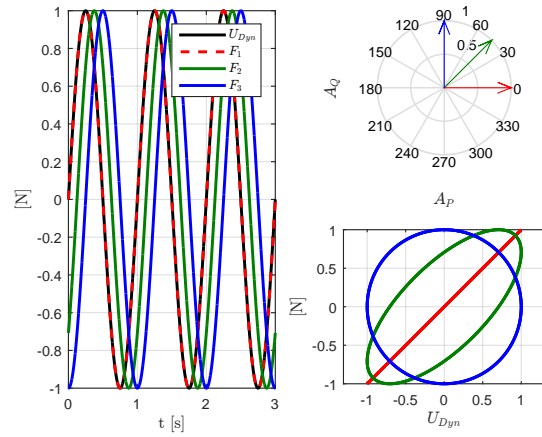

Figure 12: Simple example: effect of **quadrature** component of the aerodynamic force F_i with respect to the velocity U_{Dyn}ion

Aero	Hydro	Exp/Num	$A[m]$	$f_p[Hz]$	$\Omega[rad/s]$	$U[m/s]$	$\omega_p[rad/s]$	$f^*[-]$	$TSR[-]$	A_P [N]	A_Q [N]	$\left\|\frac{A_Q}{A_P}\right\|[-]$
Below R.	Low	E	0.10	0.25	15.71	2.33	1.57	0.067	7.96	0.979	0.0812	0.0829
		N	0.10	0.25	15.71	2.33	1.57	0.067	7.96	0.633	0.109	0.172
	Wave	E	0.01	2.10	15.71	2.33	13.1	0.057	7.96	1.066	0.109	0.102
		N	0.01	2.10	15.71	2.33	13.1	0.057	7.96	0.680	0.127	0.186
Rated	Low	E	0.10	0.25	23.04	3.67	1.57	0.043	7.41	1.413	0.163	0.115
		N	0.10	0.25	23.04	3.67	1.57	0.043	7.41	0.873	0.093	0.106
	Wave	E	0.01	2.10	23.04	3.67	13.1	0.036	7.41	1.545	0.109	0.070
		N	0.01	2.10	23.04	3.67	13.1	0.036	7.41	0.907	0.188	0.207

Table 3: Surge test results summary

Aero	Hydro	Exp/Num	$A[deg]$	$f_p[Hz]$	$\Omega[rad/s]$	$U[m/s]$	$\omega_p[rad/s]$	$f^*[-]$	$TSR[-]$	A_P [N]	A_Q [N]	$\left\|\frac{A_Q}{A_P}\right\|[-]$
Below R.	Low	E	3.00	0.65	15.71	2.33	4.08	0.151	7.96	3.257	-0.105	0.032
		N	3.00	0.65	15.71	2.33	4.08	0.151	7.96	1.594	0.257	0.161
	Wave	E	1.00	2.10	15.71	2.33	13.19	0.162	7.96	3.995	0.619	0.154
		N	1.00	2.10	15.71	2.33	13.19	0.162	7.96	1.846	0.373	0.202
Rated	Low	E	3.00	0.65	23.04	3.67	4.08	0.151	7.41	4.385	0.252	0.0575
		N	3.00	0.65	23.04	3.67	4.08	0.151	7.41	1.992	0.468	0.235
	Wave	E	1.00	2.10	23.04	3.67	13.19	0.162	7.41	5.554	-0.048	0.008
		N	1.00	2.10	23.04	3.67	13.19	0.162	7.41	3.281	0.102	0.031

Table 4: Pitch test results summary

black line refers to the experimental steady acquisitions around the nominal velocity. It can be observed that, with the setting reported in Tab.2, AeroDyn seems to be underestimating the slope of the cycles (i.e. in-phase/viscous component), see A_P in Tab.3. An indication of the areas inscribed by these hysteretic cycles is given by the ratio between quadrature (Q) and in-phase (P) component $|\frac{A_Q}{A_P}|$, reported in Tab.3 and 4, which shows comparable values for surge below rated conditions, where the discrepancy is higher for rated condition and in general for imposed pitch motion tests. Furthermore in Fig.17 and Fig.18 for surge, as well as in Fig.23 and Fig.24 for pitch, below rated and low frequency range results are reported, grouped with same amplitude but different imposed frequency. It is noticeable how for small variation in frequency, within the same wave frequency range, the unsteady aerodynamic force F_{aero}^{Dyn} is mainly changing in amplitude, keeping almost constant the in-phase/quadrature ratio parameter $|\frac{A_Q}{A_P}|$.
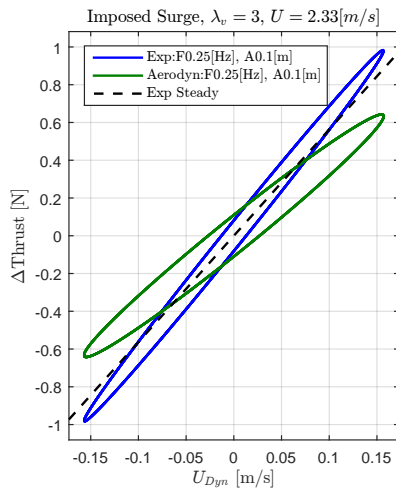
Figure 13: Experimental Vs Numerical Aerodynamic Surge Force: Low Frequency, Below Rated
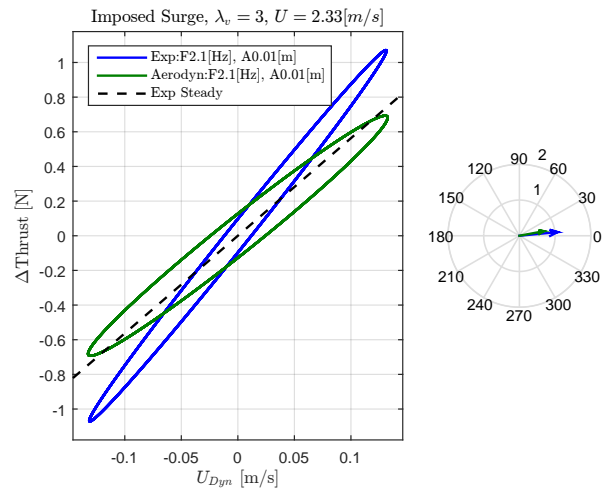

Figure 14: Experimental Vs Numerical Aerodynamic Surge Force: Wave Frequency, Below Rated
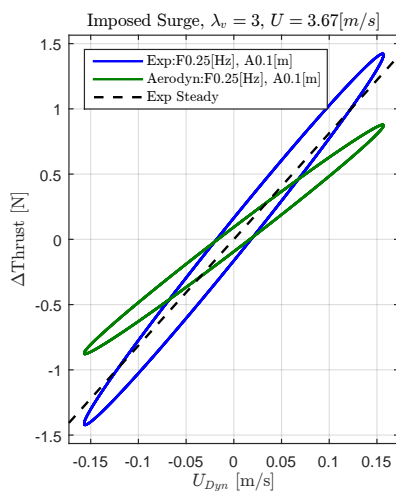

Figure 15: Experimental Vs Numerical Aerodynamic Surge Force: Low Frequency, Rated
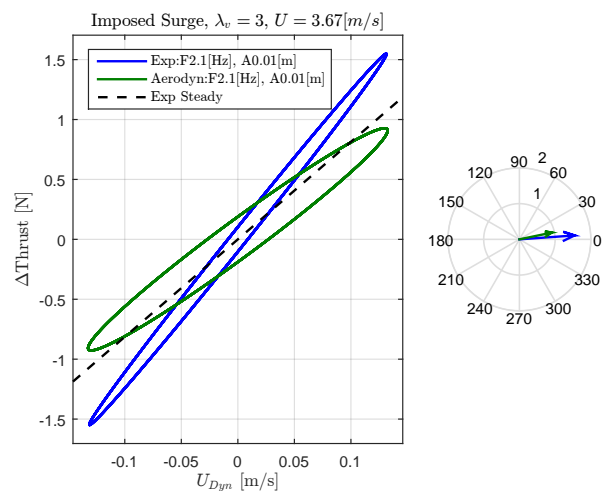

Figure 16: Experimental Vs Numerical Aerodynamic Surge Force: Wave Frequency, Rated

7. Conclusions and ongoing works

The paper presents the results of an extensive experimental campaign carried out at Politecnico di Milano Wind Tunnel, to assess the influence of substructure motion on the aerodynamics of floating offshore wind turbines. Imposed surge and pitch motions were provided to a scaled wind turbine model both a low and wave frequency and up to rated conditions. The experimental data shown hysteretic behaviours in the force Vs velocity plots, always of dissipative nature.

All the experimental tests were also run numerically in FAST-v7/AeroDyn-v13 custom environment. The experimental Vs numerical comparison has highlighted some differences. The most significant is that AeroDyn provides aerodynamic forces always with greater in-phase component A_P with respect to the dynamic velocity U_{Dyn}, as extensively described in paragraph 6.

According to the authors, the discrepancies between numerical and experimental results are to be investigated more thoroughly, since it is not straightforward to correlate them to the AeroDyn numerical implementation. Therefore, intensive experimental campaigns have been set for the summer 2016 to have a deeper insight of these phenomena based on a wider experimental database and experimental approach
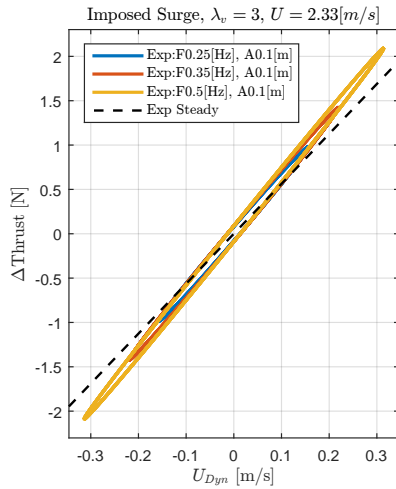
Figure 17: Surge experimental hysteretic cycles: Low Frequency constant amplitude and increasing platform frequency
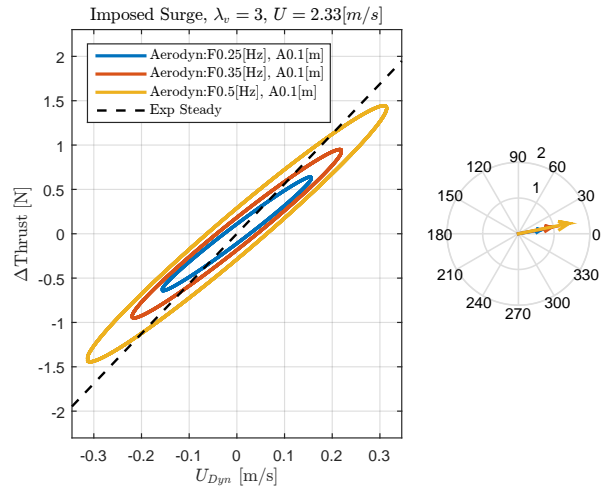
Figure 18: Surge numerical hysteretic cycles: Low Frequency constant amplitude and increasing platform frequency
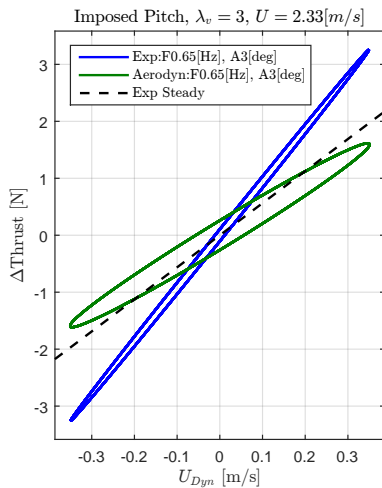

Figure 19: Experimental Vs Numerical Aerodynamic Pitch Force: Low Frequency, Below Rated
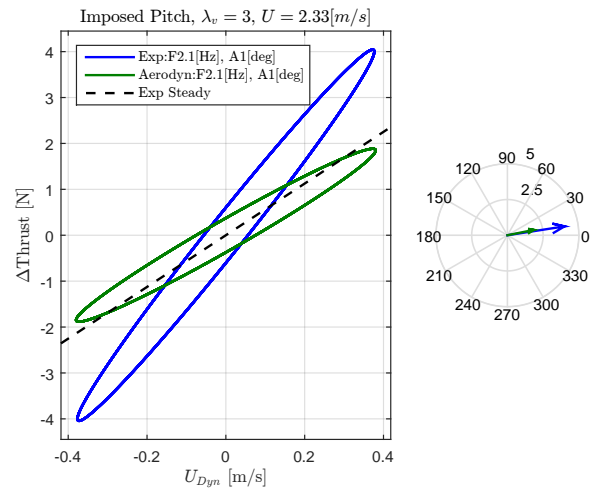
Figure 20: Experimental Vs Numerical Aerodynamic Pitch Force: Wave Frequency, Below Rated

(e.g. wake measurements). Also a sensitivity analysis on the influence of the numerical parameters (e.g. AeroDyn version, stall models etc...) on the output is being carried out.

However, as a matter of fact, the wind turbine motion affects primarily the relative velocity seen by each blade section and the overall aerodynamic force in time. This is not sufficient to explain the hysteretic results. The cause of this, which is due to unsteady aerodynamics, should be further investigated, taking into account the following issues:

- changing the wind velocity implies a variation of the angle of attack on the blade, which could induce non-linear aerodynamic behaviour

- the thrust force is also due to the wake geometry and characteristics, moving the wind turbine can induce distortion in the wake itself
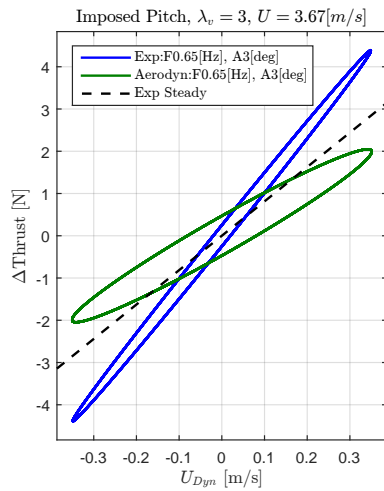
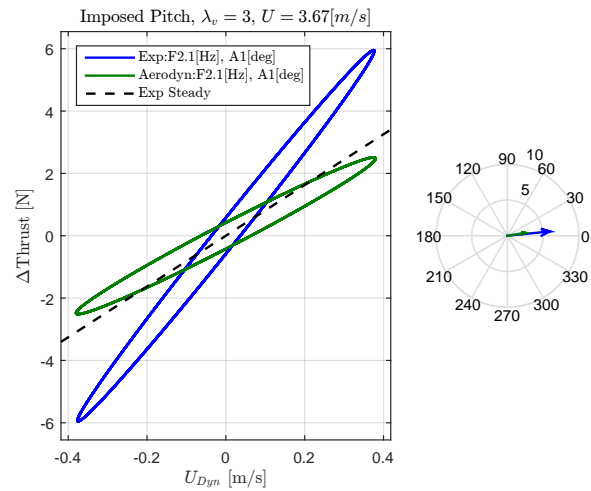Figure 21: Experimental Vs Numerical Aerodynamic Pitch Force: Low Frequency, Rated

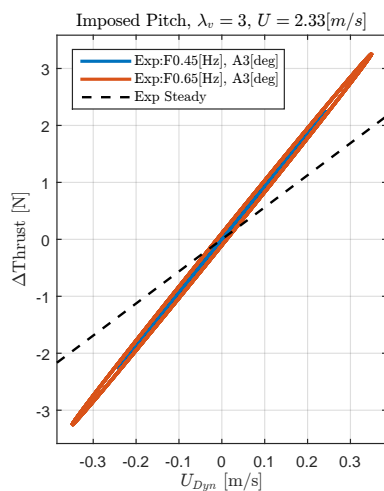Figure 22: Experimental Vs Numerical Aerodynamic Pitch Force: Wave Frequency, Rated

Figure 23: Pitch experimental hysteretic cycles: Low Frequency constant amplitude and increasing platform frequency
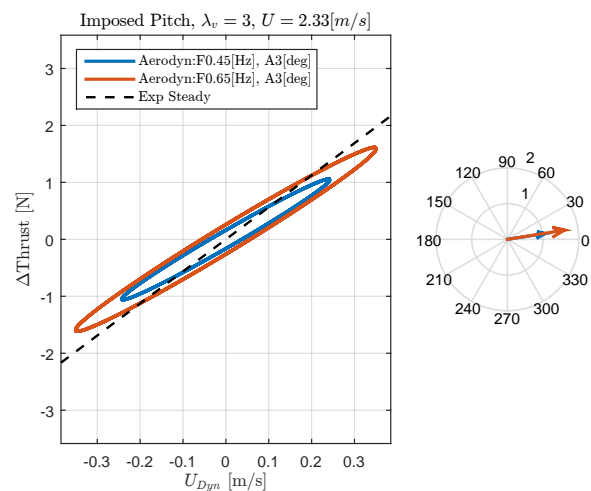

Figure 24: Pitch nsumerical hysteretic cycles: Low Frequency constant amplitude and increasing platform frequency

References

[1] C. Bak et Al, "The DTU 10-MW Reference Wind Turbine",Technical University of Denmark, DTU Wind Energy, Denmark, 2013.

[2] H2020 LIFES50+ project: `http://lifes50plus.eu/`

[3] E. Bachynski, V. Chabaud, T. Sauder, "Real-time Hybrid Model Testing of Floating Wind Turbines: Sensitivity to Limited Actuation", Energy Procedia, Volume 80, 2015.

[4] I. Bayati, M. Belloli, A. Facchinetti, and S. Giappino. "Wind tunnel tests on floating offshore wind turbines: A proposal for hardware-in-the- loop approach to validate numerical codes", Wind Engineering, 2012.

[5] I. Bayati, M. Belloli, D. Ferrari, F. Fossati, H. Giberti. "Design of a 6-DoF Robotic Platform for Wind Tunnel Tests of Floating Wind Turbines", Energy Procedia, Volume 53, 2014.

[6] I. Bayati, M. Belloli, L. Bernini, R. Mikkelsen, A. Zasso. "On the aero-elastic design of the DTU 10MW wind turbine blade for the LIFES50+ wind tunnel scale model", Journal of Physics: Conference Series, The Science of Making Torque from Wind, 2016.

[7] I. Bayati, M. Belloli, L. Bernini, E. Fiore, H.Giberti, A. Zasso, "On the functional design of the DTU10 MW

wind turbine scale model within LIFES50+ project",Journal of Physics: Conference Series, The Science of Making Torque from Wind, 2016.

[8] H. Bredmose, R. Mikkelsen, A. M. Hansen, R. Laugesen, N. Heilskov, B. Jensen, & J. Kirkegaard. "Experimental study of the DTU 10 MW wind turbine on a TLP floater in waves and wind". EWEA Offshore 2015 Conference, Copenhagen, 2015

[9] H. Bredmose, "Contribution to InnWind Deliverable 4.22, Scaling laws for Floating wind turbine testing".DTU Wind Energy. 2014.

[10] C. Bottasso, F. Campagnolo and V. Petrovic. "Wind tunnel testing of scaled wind turbine models: Beyond aerodynamics." Journal of Wind Engineering and Industrial Aerodynamics, 2014.

[11] F. Campagnolo, C. Bottasso and P. Bettini "Design, manufacturing and characterization of aero-elastically scaled wind turbine blades for testing active and passive load alleviation techniques within a ABL wind tunnel.", TORQUE, 2014.

[12] C. A. Lyon, A. P. Broeren, P. Gigure, A. Gopalarathnam, and M. S. Selig, "Summary of Low-Speed Airfoil Data, Vol. 3", SoarTech Publications, Virginia Beach, VA, 1998.

[13] G. Diana, F. Resta, A. Zasso, M. Belloli, D. Rocchi, "Forced motion and free motion aeroelastic tests on a new concept dynamometric section model of the Messina suspension bridge", Journal of Wind Engineering and Industrial Aerodynamics, Volume 92, Issue 6, May 2004.

[14] I. Bayati, J. Jonkman, A. Robertson, A. Platt, "The effects of second-order hydrodynamics on a semisubmersible floating offshore wind turbine", Journal of Physics: Conference Series, 524 (1), art. no. 012094, 2014.

[15] I. Bayati, S. Gueydon, M. Belloli, "Study of the effect of water depth on potential flow solution of the OC4 semisubmersible floating offshore wind turbine", Energy Procedia, 80, pp. 168-176, 2015.